HHS Public Access

Author manuscript

J Phys Chem Lett. Author manuscript; available in PMC 2019 August 16.

Published in final edited form as:

J Phys Chem Lett. 2018 August 16; 9(16): 4758–4764. doi:10.1021/acs.jpclett.8b02048.

First Principles Prediction of Wavelength-Dependent Product Quantum Yields

Travis Thompson and **Enrico Tapavicza**

Department of Chemistry and Biochemistry, California State University, Long Beach, 1250 Bellflower Blvd, Long Beach, CA 90840

Abstract

We present a method to predict wavelength-dependent product quantum yields (PQYs) for photochemical reactions and applied it to Z/E-isomerization and several ring-closing reactions of Z-2,5-dimethyl-1,3,5-hexatriene and truncated previtamin D. Using branching ratios from surface hopping molecular dynamics, individual trajectories are correlated with the absorption spectra of their initial structures. The wavelength-dependent PQYs are computed by dividing the average spectrum of the initial structures of the product-forming trajectories by the average spectrum of all initial structures. Accurate absorption spectra are calculated using the correlated ADC(2) method with an implicit solvent. Calculations reproduce the experimentally found trend of increasing six-ring formation and decreasing Z/E-isomerization on the red side of the spectrum. Over all seven reactions studied, the mean absolute error (MAE) between experimental and calculated PQYs (MAE) amounts to 8.1%, with the largest MAE of 18.6%. For four reactions, predicted values agree quantitatively with experiments within 5.6%.

Graphical Abstract

Enrico.Tapavicza@csulb.edu.

Supporting Information Available

Additional information of the product distribution from TDDFT-SH, computed and experimental product quantum yields of all reactions at different wavelengths.

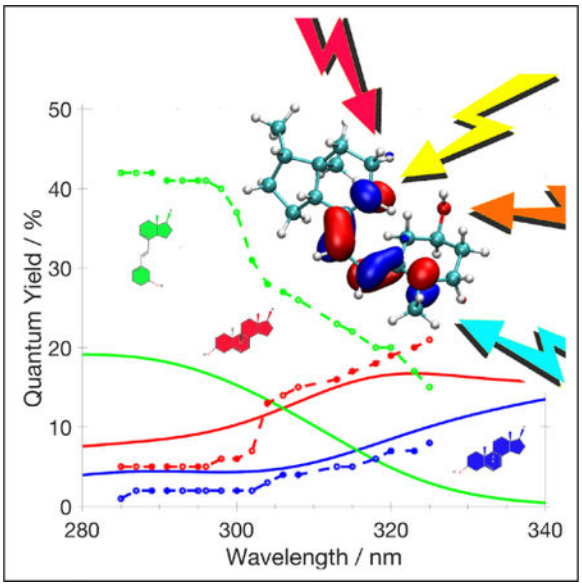

Photochemical switches offer a variety of applications for nano devices, including molecular motors and nano transistors.[1,2] Particularly interesting for these applications are systems that undergo different photochemical reactions depending on the wavelength used to induce the switching process. This has been exploited in a variety of systems.[2–6] Furthermore, the wavelength-dependent photochemistry plays a key role in the intrinsic regulation of epidermal vitamin D photosynthesis,[7] preventing vitamin D overproduction. The mechanism of this process is still under debate.[8] Several mechanisms can cause a wavelength-dependent photochemistry. On one hand, electronically excited states with different orbital character can lead to different products depending on the excitation wavelength.[9] On the other hand, the conformation adopted by a molecule can determine the product of a photochemical reaction. If the different conformers have different absorption wavelengths, a wavelength-dependent photochemistry results[10,11] (conformational control). Here, we address the latter case of conformational control. Our motivation is to develop a computational method that is able to quantitatively predict wavelength-dependent product quantum yields (PQYs) with high accuracy compared to experimental results.

The wavelength-dependent product quantum yield $\Phi(\lambda)$ of a photochemical reaction is defined[12] as the number of product molecules formed upon excitation at wavelength λ $\left(N^{\mathrm{P}}_{\mathrm{molecules}}(\lambda)\right)$ divided by the total number of photons of wavelength λ absorbed $\left(N^{\mathrm{tot}}_{\mathrm{photons}}(\lambda)\right)$:

$$\Phi(\lambda) = \frac{N^{\mathrm{P}}_{\mathrm{molecules}}(\lambda)}{N^{\mathrm{tot}}_{\mathrm{photons}}(\lambda)}. \quad (1)$$

Hence, to predict $\Phi(\lambda)$ from first principles it is necessary to know two contributions: a) the efficiency of light absorption (absorption cross section $\sigma(\lambda)$) and b) the probability that the

specific product is formed once the molecule is excited, to which we will refer to as the *branching ratio*. For conformationally flexible molecules, the macroscopic absorption cross section often strongly depends on the equilibrium distribution of conformers present in the ground state. The branching ratio of a photochemical reaction is governed by the dynamics induced by photoexcitation, which depends on the excited and ground state potential energy surfaces (PESs) and the temperature. Conformationally flexible molecules often exhibit fundamentally different photodynamics for different conformers. Thus, in order to predict wavelength-dependent PQYs, the computational approach must take into account the dependency of the molecular conformation on the absorption properties, as well as the dependency of the molecular conformation on the photodynamical behavior. The presented approach based on trajectory surface hopping is well-suited to account for both contributions. Surface hopping has been widely used to predict PQYs, but usually the raw branching rations of the simulations are simply interpreted as the quantum yields.[5,10,13–16] This interpretation only approximates the definition of the PQY (Equation 1), because the number of photons absorbed is not taken into account and the wavelength dependency of the PQYs is neglected. By specifically taking into account the relationship between product formation and absorption properties, the presented method allows to compute the PQY consistent with Equation 1 and also yields the wavelength dependency.

A detailed description of the time-dependent density functional theory (TDDFT) trajectory surface hopping (SH) method, which is based on Tully's fewest switches SH,[17] can be found elsewhere.[18] The general idea of the method is to represent the photodynamics of the macroscopic ensemble by a finite number of trajectories, where each trajectory stems from different initial conditions, e.g. nuclear coordinates and instantaneous nuclear velocities. The initial conditions are obtained from a Boltzmann ensemble at a given temperature. The nuclear degrees of freedom of each starting structure are then propagated according to Newton's equations of motion using nuclear forces evaluated for the electronically excited state using TDDFT. In addition, derivative couplings between ground and excited states are evaluated on-the-fly. The couplings describe the probability that the system decays to the ground state. Each individual simulation will follow a different trajectory and distinct reaction products may result after relaxation to the ground state. An ensemble of trajectories yields the raw product distribution or branching ratio. Since the initial structures are selected without consideration of their excitation wavelength and extinction coefficient, the branching ratio does not contain any wavelength dependency. By correlating the trajectories with the absorption spectra of their initial structures the wavelength dependency is introduced.

Using the definition of the PQY (Equation 1), we can replace number of product molecules $N^{\mathrm{P}}_{\mathrm{molecules}}(\lambda)$ by the number of photons absorbed by reactants that successfully form product $P\left(N^{\mathrm{P}}_{\mathrm{photons}}(\lambda)\right)$:

$$\Phi(\lambda) = \frac{N^{\mathrm{P}}_{\mathrm{photons}}(\lambda)}{N^{\mathrm{totons}}_{\mathrm{photons}}(\lambda)}. \quad (2)$$

This is justified assuming that one photon is needed to produce one product molecule. Considering monochromatic radiation of wavelength λ, the number of photons absorbed by a material is proportional to the oscillator strength, which is related through a line function to the absorption cross section σ(λ) or, equivalently, to the extinction coefficient $\epsilon(\lambda)$[19] Oscillator strengths for electronic transitions are routinely obtained from excited state electronic structure methods and can be converted to absorption cross sections or extinction coefficients by broadening with a line shape function. In the framework of trajectory surface hopping, $N^{\mathrm{P}}_{\mathrm{photons}}(\lambda)$ is proportional to the average absorption cross section of the initial structures that successfully produce product molecules $\sigma_P(\lambda)$:

$$N^{\mathrm{P}}_{\mathrm{photons}}(\lambda) = k\frac{1}{N^{\mathrm{P}}_{\mathrm{traj}}}\sum_{i}^{N^{\mathrm{P}}_{\mathrm{traj}}}\sigma_i(\lambda) = k\sigma_P(\lambda)\,. \quad (3)$$

$N^{\mathrm{tot}}_{\mathrm{photons}}(\lambda)$is proportional to the average absorption cross section of the initial structures of all trajectories $\sigma_{tot}(\lambda)$:

$$N^{\mathrm{tot}}_{\mathrm{photons}}(\lambda) = k\frac{1}{N^{\mathrm{tot}}_{\mathrm{traj}}}\sum_{i}^{N^{\mathrm{tot}}_{\mathrm{traj}}}\sigma_i(\lambda) = k\sigma_{tot}(\lambda)\,. \quad (4)$$

Here, k is a constant relating the number of photons to the absorption cross section, and $N^{\mathrm{P}}_{\mathrm{traj}}$ and $N^{\mathrm{tot}}_{\mathrm{traj}}$ are the number of trajectories that successfully form products and the total number of trajectories, respectively. Hence, within trajectory surface hopping, the product quantum yield can be computed as

$$\Phi(\lambda) = \frac{\frac{1}{N^{\mathrm{P}}_{\mathrm{traj}}}\sum_{i}^{N^{\mathrm{P}}_{\mathrm{traj}}}\sigma_i(\lambda)}{\frac{1}{N^{\mathrm{tot}}_{\mathrm{traj}}}\sum_{i}^{N^{\mathrm{P}}_{\mathrm{traj}}}\sigma_i(\lambda)} = \frac{\sigma_P(\lambda)}{\sigma_{tot}(\lambda)}\,. \quad (5)$$

For the practical computation of the PQY, we grouped trajectories according to their products formed. Then, for each group the average absorption spectrum $\sigma_P(\lambda)$ was computed by averaging the broadened spectra of each initial structure. Analogously, the total spectrum $\sigma_{tot}(\lambda)$ is computed by averaging the spectra of all initial structures. Using Equation 5, the PQY is computed, which avoids binning of the initial structures according to their excitation energy.

To illustrate the method, we focus on the photoproducts that arise from the photoinduced Z/E-isomerization and several electrocyclic ring-closing of Z-2,5-dimethyl-hexa-1,3,5-triene

(Z-DMHT) (Scheme 1) and truncated previtamin D (Pre) (Scheme 2), since experimentally measured wavelength-dependent PQYs are available for these molecules. The hexatriene photoactive unit, present in both molecules, is prominent to many molecular switches[2–6] and has served as model system in organic photochemistry leading to the formulation of the paradigm Non-Equilibrium of Excited State Rotamers (NEER) principle.[20,21]

The region with wavelengths larger than 240nm, for which experimental data is available for Z-DMHT and Pre, is solely governed by the first excited singlet state (S_1). Therefore, we started excited state dynamics in S_1. The product distribution of the TDDFT-SH simulations confirms the formation of the experimentally found photoproducts of Z-DMHT, for which wavelength-dependent PQYs have been measured[22] (Scheme 1). In particular, we observe Z/E-isomerization producing E-DMHT, and several ring-closing reactions, forming dimethyl-cyclohexadiene (CHD), a cyclobuten derivative (CB), and a cyclopropan derivative (CP). The first three products are formed directly in the excited state or during the transition from the excited state to the ground state, but CP is formed via a [1,6]-sigmatropic hydrogen shift at the transition from the excited state to the ground state, followed by a rearrangement in the ground state (Scheme 1). For Pre, the main photochemical products (Scheme 2) are tachysterol (Tachy), resulting from Z/E-isomerization, and the two isomers, lumisterol (Lumi) and provitamin D (Pro), resulting from six-ring formation. The found products of Pre are also consistent with the major products found in experiments.[23,24] Besides, we also find a large number of unreactive trajectories and a few other minor products (Table S1, Figure S1, Figure S2) in both molecules.

To obtain the wavelength-dependent PQYs, we computed the ten lowest excitation energies and oscillator strengths of the initial structures of the TDDFT-SH simulations using TDDFT with the PBE0 approximation[25] (TDPBE0) and the algebraic diagrammatic construction through second-order (ADC(2)) method[26] in combination with the COSMO implicit solvent model.[27,28] Figure 1 and 2 confirm that the long-wavelength region beyond 240nm is solely governed by S_1. Furthermore, the magnitudes and distribution of the S_1 oscillator strengths varies if we group them according to the photoproduct that is formed by the corresponding trajectory. Notably, the subset of structures that form the cyclohexadiene derivatives CHD, Pro, and Lumi exhibit excitation energies that reach further into the red side of the spectrum than the structures that lead to Z/E-isomerization. To obtain smooth absorption spectra, we used a Gaussian line shape to convert oscillator strengths to extinction coefficients (panels A of Figures 3 and 4). The peak positions (λ_{max}) of the ADC(2) total absorption spectra agree within 3nm with the experimentally measured spectra for both, Z-DMHT and Pre. The λ_{max} values computed by TDPBE0 are red-shifted by 29 and 30nm with respect to the experimental values, for Z-DMHT and Pre, respectively (panels A of Figures S3 and S4). Because of the more accurate spectra of ADC(2) compared to TDPBE0, we present here PQYs computed by ADC(2); TDPBE0 results are given in the Supporting Information (SI). In addition to the total absorption spectra, we computed the absorption spectra of the subset of trajectories that form a given product (Figure 3, A and Figure 4, A).

Dividing the spectra of the product-forming trajectories by the total absorption spectra (Equation 5), we obtain the wavelength-dependent PQYs for the reactions of Z-DMHT (Figure 3, B) and Pre (Figure 4, B). Computed values, mean errors (ME), and mean absolute

errors (MAE) with respect to experimental values are given in the SI (Tables S2–S5). The PQYs of E-DMHT formation (Φ_E) and CHD formation (Φ_{CHD}) (Figure 3, B) agree well with the experimentally measured values. In particular, the decrease of Φ_E and the increase of Φ_{CHD} on the red side of the experimental spectrum between 290nm and 303nm is well reproduced by the calculations. The MAE between calculated and experimental values are 5.5% and 12.0%, for Φ_{CHD} and Φ_E, respectively. Also the PQYs of CB formation agree well with the experimentally measured value and are underestimated by only 3% on average. For the CP formation, calculations overestimate the PQYs by a larger amount of about 12.9% on average. The agreement of TDPBE0 PQYs with experimental values is similar to ADC(2) (Figures S3 and S4, Tables S3 and S7 -S9), but we should keep in mind that the curves of the PQYs (Figures S3 and S4) should be red-shifted by about 30nm to compensate the error in the spectra.

The PQYs for the conversion of Pre to Lumi (Φ_{Lumi}) and Pro (Φ_{Pro}) quantitatively agree with the experimentally measured values over the whole spectrum where experimental data is available. MAEs between experimentally measured and calculated values are 2.9% and 2.0% for Lumi and Pro formation, respectively. The experimentally found increase of Φ_{Lumi} and Φ_{Pro} on the red side of the spectrum is also well reproduced by the calculations. The deviation between experiment and calculation is larger for Tachy formation (Φ_{Tachy}); here, calculations underestimate experimental values by 18.6% on average. Qualitatively, however, the calculations confirm the experimentally found decrease of Φ_{Tachy} with increasing wavelength.

We implemented a method based on TDDFT-SH and ADC(2) absorption spectra to compute wavelength-dependent product quantum yields (PQYs) and applied it to the Z/E-isomerization and ring-closing reactions of Z-DMHT and Pre. Over all available data points of the seven reactions studied, the mean absolute error between experimentally measured and calculated PQYs (MAE) amounts to 8.1%. For four reactions, the predicted PQYs agree quantitatively within 5.6% with the experimentally measured values. For E-DMHT and CP formation, the agreement with experiments is better than 13% and for Tachy formation we find the largest error of 18.6%. The experimentally found trend of increasing six-ring formation and decreasing Z/E-isomerization with increasing wavelength is correctly reproduced by the calculations. The good accuracy of the method is to one part due to the high accuracy of the computed absorption spectra, but it also shows the predictive power of the TDDFT-SH method, despite its approximative nature.

Potential sources of errors in our calculations possibly arise from the neglect of the solvent, in both the generation of the Boltzmann ensembles as well as in the excited state SH simulations. In the spectra calculations, the solvent has been approximated by an electrostatic continuum. Approximations introduced by the use of TDDFT and the approximate hybrid exchange-correlation functional possibly affect the accuracy of the branching ratio due to erroneous description of conical intersections or the neglect of double excitations[29,30] during excited state dynamics.

However, an appealing factor of our method is that it is easily extendible by step-wise improvements to achieve higher accuracy. For instance, explicit solvent molecules could be

included in ground and excited state simulations using a hybrid quantum mechanical/molecular mechanics[31,32] or even a full quantum[33] approach. Furthermore, the quantum nature of the nuclei could be considered in the initial sampling by either using a Wigner distribution[34] or path-integral molecular dynamics.[35] More accurate branching ratios could possibly be computed using correlated wavefunction based electronic structure methods,[32,36–38] if the increased computational cost is affordable. Lastly, the accuracy of absorption spectra could further be improved by taking into account vibronic effects[39,40] and effects of an explicit solvent.[40] To include reactions of higher excited states, the method can be extended by starting dynamics in higher excited states.

Overall the present method constitutes an efficient tool to predict wavelength-dependent PQYs in conformationally controlled photochemical reactions. The method can be applied to assist the design and optimization of photochemical switches.

Computational Details

We use *ab-initio* molecular dynamics (AIMD)[41] to sample the ground-state ensemble and to model photodynamics of the molecules. All AIMD simulations were performed with the density functional theory (DFT)[42] and TDDFT[43] modules of the TURBOMOLE V6.3.[44] Simulations employ the def2-SVP[45] basis set. *Ab initio* Replica exchange molecular dynamics (REMD)[11,46] is used to enhance the sampling of ground state molecular conformations and employ the PBE functional,[47] accelerated using the resolution of identity approximation.[48] REMD was performed in the canonical ensemble at four temperatures (300K, 600K, 900K, 1200K) controlled by a Nosé-Hoover thermostat.[49,50] Switches between the trajectories at different temperatures were evaluated every 200 molecular dynamics steps. A time step of 50 au was used to propagate the nuclear degrees of freedom. Non-adiabatic molecular dynamics simulations were carried out with the TDDFT-SH method[51] as implemented in TURBOMOLE.[10,18] From the ground-state Boltzmann ensemble at 300K generated by REMD, we sequentially choose several hundreds of snapshot structures (Z-DMHT: 991, Pre: 684) and their instantaneous velocities every 80 time steps (96.7fs) as starting geometry for an excited state dynamics simulation. Initial structures were propagated in the photochemically active S_1 state. The PBE0 approximation to the exchange-correlation functional[25] was used in TDDFT-SH simulations, since it produces accurate PES for hexatriene systems.[10] To minimize problems with instabilities at conical intersections,[9,30] we used the Tamm-Dancoff approximation.[52] Each TDDFT-SH simulation was propagated for 900fs allowing the full excited-state decay and subsequent hot ground-state reactions of each molecule. The total energy was conserved in TDDFT-SH simulations (NVE ensemble). The ten lowest singlet excitation energies and oscillator strengths were calculated for each initial structure of the trajectories by ADC(2)[26] and TDPBE0. ADC(2) was applied within the resolution of identity approximation,[53,54] employing the def2-TZVP basis set,[45] as previously described.[55] TDPBE0 calculations make use of the full linear response and the def2-SVP basis.[45] Oscillator strengths were converted into molar decadic extinction coefficients by broadening with a Gaussian function with a full width at half maximum of 0.15eV and averaged to obtain the macroscopic absorption spectrum.[39,56] The conductor-like screening (COSMO) model was used in

ADC(2) calculations to account for solvent effects;[27,28] a dielectricity constant of 1.844 and a refractive index of 1.3575, corresponding to n-pentane at 20°C was used.[57]

Supplementary Material

Refer to Web version on PubMed Central for supplementary material.

Acknowledgement

Research reported in this article was supported by National Institute of General Medical Sciences of the National Institutes of Health (NIH) under award numbers R15GM126524, UL1GM118979–02, TL4GM118980, and RL5GM118978. The content is solely the responsibility of the authors and does not necessarily represent the official views of the NIH. We also acknowledge financial support of the U.S. Department of Education grant number P031M140050. We acknowledge technical support from the Division of Information Technology of CSULB.

References

(1). Feringa BL The Art of Building Small: From Molecular Switches to Motors (Nobel Lecture). Angew. Chem. Intl. Ed 2017, 56, 11060–11078.

(2). Rangel NL; Williams KS; Seminario JM Light-activated molecular conductivity in the photoreactions of vitamin D3. J. Phys. Chem. A 2009, 113, 6740–6744. [PubMed: 19514787]

(3). Natarajan LV; Tondiglia V; Bunning TJ; Crane RL; Adams WW Liquid crystalline siloxanes containing spiropyran chromophores as reversible optical data storage materials. Adv. Mater. Opt. Electr 1992, 1, 293–297.

(4). Rogers RA; Rodier AR; Stanley JA; Douglas NA; Li X; Brittain WJ A study of the spiropyran-merocyanine system using ion mobility-mass spectrometry: experimental support for the cisoid conformation. Chem. Commun 2014, 50, 3424–3426.

(5). Wiebeler C; Bader CA; Meier C; Schumacher S Optical spectrum, perceived color, refractive index, and non-adiabatic dynamics of the photochromic diarylethene CMTE. Phys. Chem. Chem. Phys 2014,

(6). Siewertsen R; Strübe F; Mattay J; Renth F; Temps F Tuning of switching properties and excited-state dynamics of fulgides by structural modifications. Phys. Chem. Chem. Phys 2011, 13, 3800–3808. [PubMed: 21210030]

(7). MacLaughlin J; Anderson R; Holick M Spectral character of sunlight modulates photosynthesis of previtamin D3 and its photoisomers in human skin. Science 1982, 216, 1001–1003. [PubMed: 6281884]

(8). van Dijk A; den Outer P; van Kranen H; Slaper H The action spectrum for vitamin D3: initial skin reaction and prolonged exposure. Photochem. Photobiol. Sci 2016, 15, 896–909. [PubMed: 27286277]

(9). Tapavicza E; Tavernelli I; Rothlisberger U; Filippi C; Casida ME Mixed timedependent density-functional theory/classical trajectory surface hopping study of oxirane photochemistry. J. Chem. Phys 2008, 129, 124108. [PubMed: 19045007]

(10). Tapavicza E; Meyer AM; Furche F Unravelling the details of vitamin D photosynthesis by non-adiabatic molecular dynamics simulations. Phys. Chem. Chem. Phys 2011, 13, 20986. [PubMed: 22020179]

(11). Cisneros C; Thompson T; Baluyot N; Smith AC; Tapavicza E The role of tachysterol in vitamin D photosynthesis - a non-adiabatic molecular dynamics study. Phys. Chem. Chem. Phys. 2017, 19, 5763–5777. [PubMed: 28105477]

(12). Braslavsky SE Glossary of terms used in photochemistry, (IUPAC Recommendations 2006). Pure Appl. Chem 2007, 79, 293–465.

(13). Böckmann M; Doltsinis NL; Marx D Enhanced photoswitching of bridged azobenzene studied by nonadiabatic ab initio simulation. J. Chem. Phys 2012, 137, 22A505.

(14). Vincent JC; Muuronen M; Pearce KC; Mohanam LN; Tapavicza E; Furche F That Little Extra Kick: Nonadiabatic Effects in Acetaldehyde Photodissociation. J. Phys. Chem. Lett 2016, 7, 4185–4190.

(15). Schalk O; Geng T; Thompson T; Baluyot N; Thomas RD; Tapavicza E; Hansson T Cyclohexadiene Revisited: A Time-Resolved Photoelectron Spectroscopy and ab Initio Study. J. Phys. Chem. A 2016, 120, 2320. [PubMed: 27018427]

(16). Shemesh D; Gerber RB Molecular Dynamics of Photoinduced Reactions of Acrylic Acid: Products, Mechanisms, and Comparison with Experiment. J. Phys. Chem. Lett 2018, 9, 527–533. [PubMed: 29325414]

(17). Tully JC Molecular Dynamics with Electronic Transitions. J. Chem. Phys 1990, 93, 1061.

(18). Tapavicza E; Bellchambers GD; Vincent JC; Furche F Ab initio non-adiabatic molecular dynamics. Phys. Chem. Chem. Phys 2013, 15, 18336–18348. [PubMed: 24068257]

(19). Hilborn RC Einstein coefficients, cross sections, f values, dipole moments, and all that. Am. J. Phys 1982, 50, 982–986.

(20). Vroegop P; Lugtenburg J; Havinga E Conformational equilibrium and photochemistry of hexa-1,3,5-trienes. Tetrahedron 1973, 29, 1393–1398.

(21). Whitesell JK; Minton MA; Tran VD The non-equilibration of excited rotamers (NEER) principle. Ground-state conformational bias in triene photocyclizations. J. Am. Chem. Soc 1989, 111, 1473–1476.

(22). Brouwer A; Cornelisse J; Jacobs H Wavelength effect on the photochemical reactions of (z)-2,5-dimethyl-1,3,5-hexatrene: selective excitation of rotamers. Tetrahedron 1987, 43, 435–438.

(23). Havinga E Vitamin D, example and challenge. Experientia 1973, 29, 1181–1193. [PubMed: 4758912]

(24). Dauben WG; Disanayaka B; Funhoff DJH; Zhou B; Kohler BE; Schilke DE Polyene 21Ag and 11Bu states and the photochemistry of previtamin D3. J. Am. Chem. Soc 1991, 113, 8367–8374.

(25). Perdew JP; Ernzerhof M; Burke K Rationale for mixing exact exchange with density functional approximations. J. Chem. Phys 1996, 105, 9982–9985.

(26). Schirmer J Beyond the random-phase approximation: A new approximation scheme for the polarization propagator. Phys. Rev. A 1982, 26, 2395.

(27). Schürmann AKG COSMO: A new approach to dielectric screening in solvents with explicit expressions for the screening energy and its gradient. J. Chem. Soc. Perkin Trans.2 1993, 5, 799–805.

(28). Lunkenheimer B; Köhn A Solvent effects on electronically excited states using the conductor-like screening model and the second-order correlated method ADC (2). J. Chem. Theory Comput 2012, 9, 977–994. [PubMed: 26588741]

(29). Maitra NT; Zhang F; Cave RJ; Burke K Double excitations within timedependent density functional theory linear response. J. Chem. Phys 2004, 120, 5932–5937. [PubMed: 15267474]

(30). Levine BG; Ko C; Quenneville J; Martinez TJ Conical intersections and double excitations in density functional theory. Mol. Phys 2006, 104, 10391051.

(31). Laio A; VandeVondele J; Rothlisberger U A Hamiltonian electrostatic coupling scheme for hybrid Car–Parrinello molecular dynamics simulations. J. Chem. Phys 2002, 116, 6941–6947.

(32). Ruckenbauer M; Barbatti M; Mller T; Lischka H Nonadiabatic Photodynamics of a Retinal Model in Polar and Nonpolar Environment. J. Phys. Chem. A 2013, 117, 2790–2799. [PubMed: 23470211]

(33). Provorse Long MR; Isborn CM Combining Explicit Quantum Solvent with a Polarizable Continuum Model. J. Phys. Chem. B 2017, 121, 10105–10117. [PubMed: 28992689]

(34). Wigner EP Part I: Physical Chemistry Part II: Solid State Physics; Springer, Berlin, Heidelberg, 1997; pp 110–120.

(35). Craig IR; Manolopoulos DE Quantum statistics and classical mechanics: Real time correlation functions from ring polymer molecular dynamics. J. Chem. Phys 2004, 121, 3368–3373. [PubMed: 15303899]

(36). Tapavicza E; Tavernelli I; Rothlisberger U Ab Initio Excited State Properties and Dynamics of a Prototype σ-Bridged-Donor-Acceptor Molecule. J. Phys. Chem. A 2009, 113, 9595–9602. [PubMed: 19663389]

(37). Herbert JM; Zhang X; Morrison AF; Liu J Beyond Time-Dependent Density Functional Theory Using Only Single Excitations: Methods for Computational Studies of Excited States in Complex Systems. Acc. Chem. Res 2016, 49, 931–941. [PubMed: 27100899]

(38). Park JW; Shiozaki T On-the-Fly CASPT2 Surface-Hopping Dynamics. J. Chem. Theory Comput 2017, 13, 3676–3683. [PubMed: 28686839]

(39). Tapavicza E; Furche F; Sundholm D Importance of vibronic effects in the UV-Vis spectrum of the 7, 7, 8, 8-tetracyanoquinodimethane anion. J. Chem. Theory Comput 2016, 12, 5058–5066. [PubMed: 27585186]

(40). Zuehlsdorff TJ; Isborn CM Combining the ensemble and Franck-Condon approaches for calculating spectral shapes of molecules in solution. J. Chem. Phys 2018, 148, 024110. [PubMed: 29331131]

(41). Elliott SD; Ahlrichs R; Hampe O; Kappes MM Auto-ionised products from the reaction of sodium clusters with dioxygen: Theory and experiment. Phys. Chem. Chem. Phys 2000, 2, 3415–3424.

(42). Häser M; Ahlrichs R Improvements on the direct SCF method. J. Comput. Chem 1989, 10, 104–111.

(43). Furche F; Ahlrichs R Adiabatic time-dependent density functional methods for excited state properties. J. Chem. Phys 2002, 117, 7433–7447.

(44). Furche F; Ahlrichs R; Hättig C; Klopper W; Sierka M; Weigend F Turbomole. WIREs: Comput. Mol. Sci 2014, 4, 91100.

(45). Schäfer A; Horn H; Ahlrichs R Fully optimized contracted Gaussian basis sets for atoms Li to Kr. J. Chem. Phys 1992, 97, 2571–2577.

(46). Sugita Y; Okamoto Y Replica-exchange molecular dynamics method for protein folding. Chem. Phys. Lett 1999, 314, 141–151.

(47). Perdew J; Burke K; Ernzerhof M Generalized gradient approximation made simple. Phys. Rev. Lett 1996, 77, 3865. [PubMed: 10062328]

(48). Eichkorn K; Weigend F; Treutler O; Ahlrichs R Auxiliary basis sets for main row atoms and transition metals and their use to approximate Coulomb potentials. Theor. Chem. Acc 1997, 97, 119–124.

(49). Nosé S A molecular dynamics method for simulations in the canonical ensemble. Mol. Phys 1984, 52, 255–268.

(50). Hoover W Canonical dynamics: equilibrium phase-space distributions. Phys. Rev. A 1985, 31, 1695.

(51). Tapavicza E; Tavernelli I; Rothlisberger U Trajectory surface hopping within linear response time-dependent density-functional theory. Phys. Rev. Lett 2007, 98, 023001. [PubMed: 17358601]

(52). Hirata S; Head-Gordon M Time-dependent density functional theory within the Tamm-Dancoff approximation. Chem. Phys. Lett 1999, 314, 291–299.

(53). Christiansen O; Koch H; Jørgensen P The 2nd-order approximate coupled-cluster singles and doubles model cc2. Chem. Phys. Lett 1995, 243, 409–418.

(54). Hättig C; Köhn A Transition moments and excited-state first-order properties in the coupled-cluster model CC2 using the resolution-of-the-identity approximation. J. Chem. Phys 2002, 117, 6939–6951.

(55). De Haan DO; Tapavicza E; Riva M; Cui T; Surratt JD; Smith AC; Jordan M-C; Nilakantan S; Almodovar M; Stewart TN et al. Nitrogen-Containing, Light-Absorbing Oligomers Produced in Aerosol Particles Exposed to Methylglyoxal, Photolysis, and Cloud Cycling. Environ. Sci. & Technol 2018, 52, 4061–4071. [PubMed: 29510022]

(56). Epstein SA; Tapavicza E; Furche F; Nizkorodov SA Direct photolysis of carbonyl compounds dissolved in cloud and fog droplets. Atmos. Chem. Phys 2013, 13, 9461–9477.

(57). Speight JG Lange's handbook of chemistry; McGraw-Hill New York, 2005; Vol. 1.

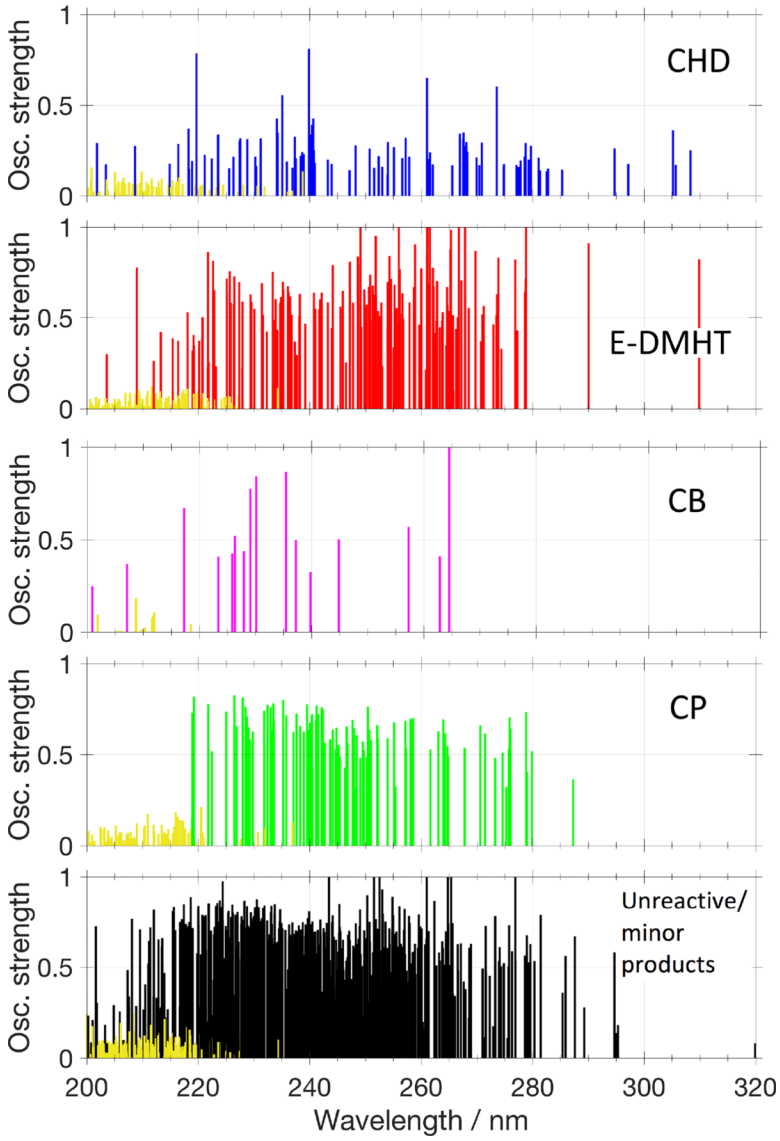

Figure 1:

Distribution of the ADC(2) oscillator strengths of the first excited singlet state of the initial structures (blue, red, magenta, green, black) of the Z-DMHT trajectories that form the indicated product. Yellow: oscillator strengths of the second excited singlet state.

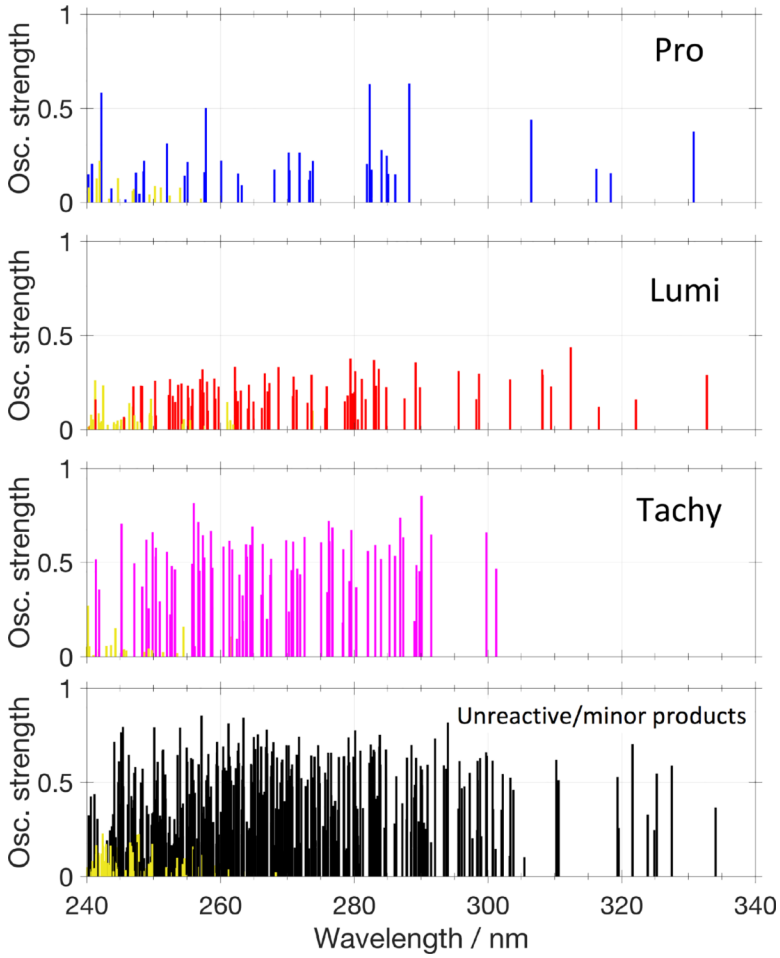

Figure 2:
Distribution of the ADC(2) oscillator strengths of the first excited singlet state of the initial structures of the Pre trajectories that form the indicated product (blue, red, magenta, black). Yellow: oscillator strengths of the second excited singlet state.

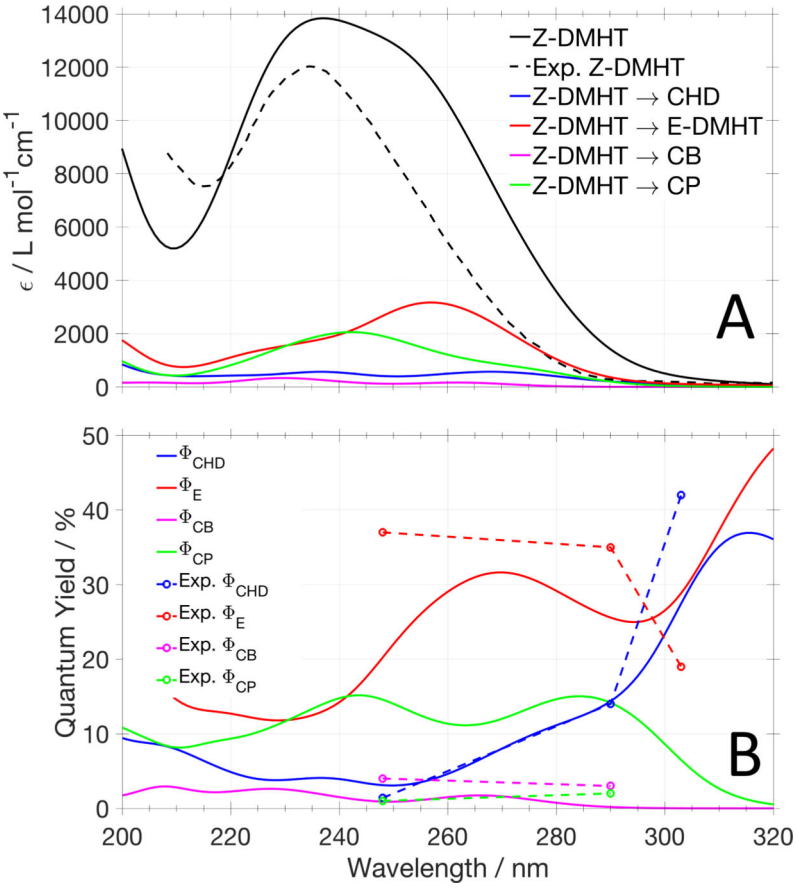

Figure 3:

A: Absorption spectra of Z-DMHT. The calculated absorption spectrum of Z-DMHT of all TDDFT-SH initial structures (solid) and experimentally measured spectrum[22] (dashed) are shown in black. The spectra of the initial structures of the trajectories that lead to the indicated reactions are given in color. B: Calculated and experimentally measured[22] (Exp.) wavelength-dependent product quantum yields of E-DMHT (Φ_E), CHD (Φ_{CHD}), CB (Φ_{CB}), and CP (Φ_{CP}).

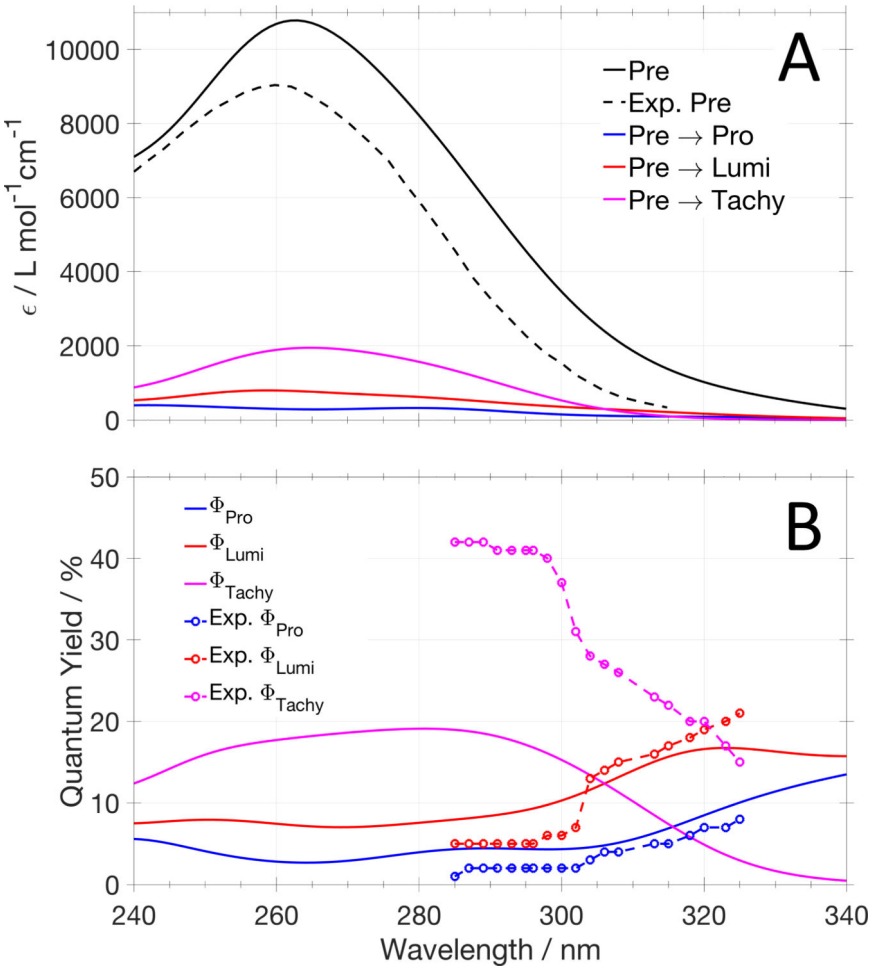

Figure 4:

A: Absorption spectra of Pre. Calculated spectrum of all TDDFT-SH initial structures (solid) and experimentally measured spectrum[24] (dashed) are shown in black. The spectra of the initial structures of the trajectories that lead to the indicated reactions are given in color. B: Calculated and experimentally measured[24] (Exp.) wavelength dependent product quantum yields of Pre[24] wavelength-dependent product quantum yields of Lumi (Φ_{Lumi}), Pro (Φ_{Pro}), and Tachy (Φ_{Tachy}).

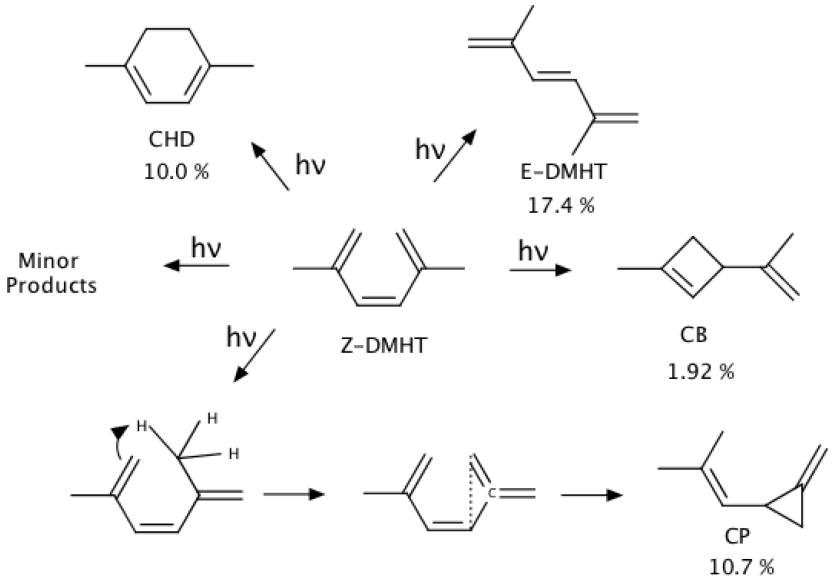

Scheme 1:

Major photoproducts of Z-DMHT observed in experiments[22] and confirmed by TDDFT-SH simulations. For CP, the mechanism of its formation found in simulations is indicated. Raw branching ratios from simulations are indicated for the products.

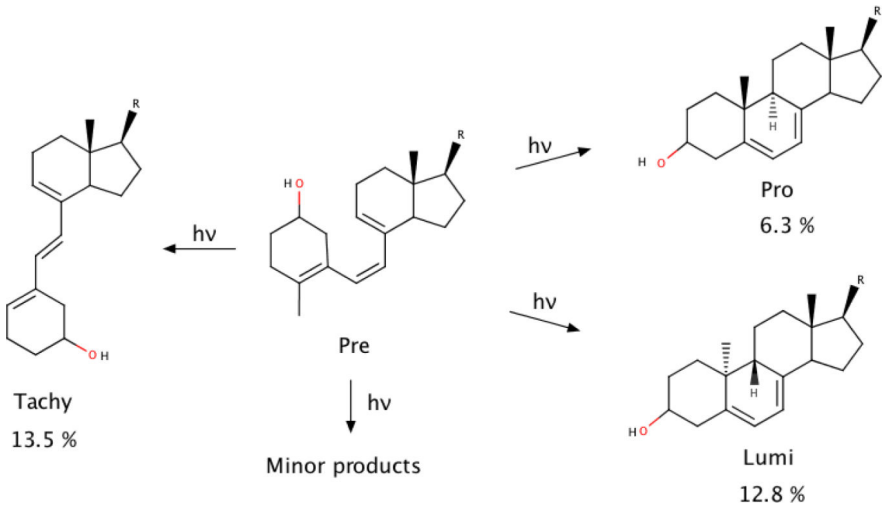

Scheme 2:

Major reactions and their products observed in TDDFT-SH simulations of Pre. The aliphatic chain (R) has been replaced by a methyl group in our calculations. Z/Eisomerization, forming tachysterol (left) and ring-closing reactions, forming lumisterol and provitamin D (right). Raw branching ratios from simulations are indicated for the products.